

Highly photo-stable Perovskite nanocubes: towards integrated single photon sources based on tapered nanofibers

Stefano Pierini,^{†,‡} Marianna D'Amato,[‡] Mayank Goyal,^{¶,§} Quentin Glorieux,[‡]
Elisabeth Giacobino,[‡] Emmanuel Lhuillier,[¶] Christophe Couteau,[†] and Alberto
Bramati^{*,‡}

[†]*Laboratory Light, nanomaterials & nanotechnologies L2n, University of Technology of
Troyes & CNRS ERL 7004, 12 rue Marie Curie, 10000 Troyes, France*

[‡]*Laboratoire Kastler Brossel, Sorbonne Université, CNRS, ENS-PSL Research University,
Collège de France, 4 place Jussieu, 75252 Paris Cedex 05, France*

[¶]*Sorbonne Universit, CNRS - UMR 7588, Institut des NanoSciences de Paris, INSP,
F-75005 Paris, France*

[§]*Department of Chemistry, Indian Institute of Science Education and Research (IISER),
Pune 411008, India*

E-mail: alberto.bramati@lkb.upmc.fr

Abstract

The interest in perovskite nanocrystals (NCs) such as CsPbBr₃ for quantum applications is rapidly raising, as it has been demonstrated that they can behave as very efficient single photon emitters. The main problem to tackle in this context is their photo-stability under optical excitation. In this article, we present a full analysis of the optical and quantum properties of highly efficient perovskite nanocubes synthesized with an established method, which is used for the first time to produce quantum emitters, and is shown to ensure an increased photo-stability. These emitters exhibit reduced blinking together with a strong photon antibunching. Remarkably these features are hardly affected by the increase of the excitation intensity well above the emission saturation levels. Finally, we achieve for the first time the coupling of a single perovskite nanocube with a tapered optical nanofiber in order to aim for a compact integrated single photon source for future applications.

Keywords

perovskites, single photon sources, quantum dots, nanocrystals, nanofibers

The interest in perovskites, originally studied for solar-cell applications,¹ has recently increased in the quantum optics community. Perovskite nanocrystals are indeed versatile emitters and the possibility to tune their emission wavelength playing on their size and composition, together with their coherent emission² and their ability to obtain single photon emission at low^{3,4} and room⁵ temperatures makes them promising nano-objects for quantum applications. Despite these strong points,⁶ the optical stability is still the main limitation in their use as they usually bleach after few minutes under illumination. Multiple approaches have been attempted to reduce this problem such as polymer encapsulation,^{7,8} but also alumina encapsulation using atomic layer deposition,^{9,10} and

surface passivation.¹¹ Although these methods have shown some effects in reducing the bleaching, only partial results are achieved. Indeed, the first technique is not suitable for applications such as the coupling of single emitters with photonic devices, as it requires the NCs to be surrounded by a dense polymer matrix. The second technique is more promising, however no single photon emission has been demonstrated so far using this method.

We report here a method of fabrication, used for the first time for this purpose, that allows us to obtain higher stability samples of perovskite nanocrystals which can be excited under optical excitation for more than one hour. We also investigate the role of the dilution on the stability, suggesting new approaches to address this problem. Thanks to this improved stability, we were able to perform a full characterization of the optical and quantum features of perovskite nanocrystals, showing at the same time reduced blinking and strong photon antibunching of the emission. Finally, for the first time with such kind of emitters, we achieve the coupling of a single perovskite nanocrystal with a tapered optical nanofiber. As it has been shown with atoms^{12,13} and solid state emitters¹⁴⁻¹⁷ this technique is of paramount importance for applications in the emerging field of quantum technologies. Our result is a promising step towards the realization of a compact integrated single photon device at room temperature with perovskite nanoemitters.

Perovskite nanocubes fabrication

We start by describing the growth method of nanocrystals of CsPbBr₃ presenting a bright green photoluminescence (PL) (see Figure 3a) around 500 nm. The usual procedure as described by Protecescu *et al.*¹⁸ leads to bright nanoparticles, however they appear to be difficult to use for single emitter photonic applications due to a limited colloidal stability under dilute condition. The alkyl ammonium ligands have strong binding dynamics¹⁹ to the nanocrystals surface which reduce their stabil-

ity under dilute condition. It was recently proposed to use alternative ligands such as zwitterion²⁰ or phosphonic acid²¹ to enhance the binding of the ligand and overcome the loss of stability under dilution. Here, we explore a different approach to obtain nanocrystals more stable under dilute condition. We use a procedure initially developed for the growth of CsPbBr₃ nanosheet.²² Compared to Protecescu *et al.*¹⁸ there are three major changes:

1. less caesium oleate is introduced to favor the growth of Cs free phase.
2. two additional ligands with saturated alkyl chains are introduced (octanoic acid and octyl amine) to favor the crystallization of the Cs free phase.
3. the reaction time is extended from 30 s to 35 min to favor the reaction step.

In this synthesis, the main product is CsPbBr₃ nanoplatelets²³ and presents an absorption peak at 430 nm as shown in Figure 1a. Moreover, there are two additional products, the first one is made of Cs-free nanoplatelets where a plane of lead bromide is sandwiched between two planes of ligands with C8 chains. This phase presents a clear peak at 398 nm in the absorption spectrum.²³ The second one is composed of synthesized cubes responsible for the small absorption edge around 510 nm, and it is actually the one we are interested in. We can see its signature as a small change in the slope of the absorption curve, visible in the inset of Figure 1a.

It turns out that these nanocubes, despite the fact that they are a side product of the synthesis, are very interesting for single photon emitters as we will show. In the following, we select only the PL from these cubes. Almost all the CsPbBr₃ nanoplatelets are removed by centrifuging the solution as explained in methods. The obtained CsPbBr₃ nanocubes appear to be more stable upon dilution than the one obtained by the direct procedure, as shown in the following.

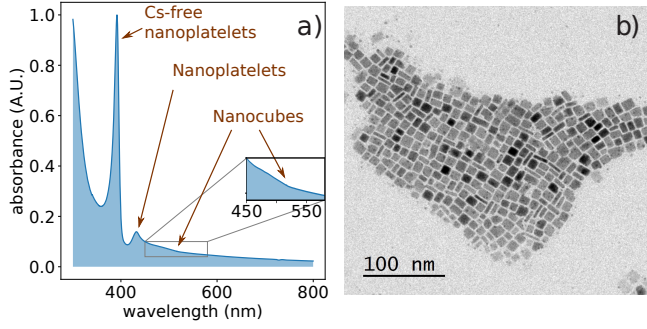


Figure 1: a) Absorption spectrum of the products obtained from the synthesis with the method described in the text before the last centrifugation. The contribution of the three phases is evidenced. The inset shows the portion of the spectrum corresponding to nanocubes contribution. b) Transmission electron microscopy image of CsPbBr₃ nanocubes responsible for the photoluminescence.

Optical characterization

We optically characterized the NCs using an inverted confocal microscope: the experimental setup is shown in Figure 2a.

The samples are prepared for optical characterization measurements by spin-coating the colloidal solution on a glass coverslip. A LED lamp at 400 nm is first used to locate the emitters and an image of the field of view of the microscope is collected by a CMOS camera. A single emitter is then excited via a 405 nm picosecond pulsed laser (pulse width < 50 ps) with a repetition rate adjustable from 2.5 MHz to 5 MHz. After filtering out the excitation wavelength, the luminescence of a single perovskite nanocube is collected by an inverted confocal microscope and sent to the optical characterization part. All the measurements were performed at room temperature.

A typical emission spectrum is reported in Figure 3a and shows a central wavelength of 500 nm with a full width at half maximum (FWHM) of about 15 nm. The distribution of the emitted wavelengths with the corresponding FWHM is shown in Figure 3b for 78 emitters.

Here, we clearly see two main peaks with central emission wavelength (CEW) at 485 nm and 510 nm respectively. The mean FWHM of the emitted light is about 14 nm for the first peak

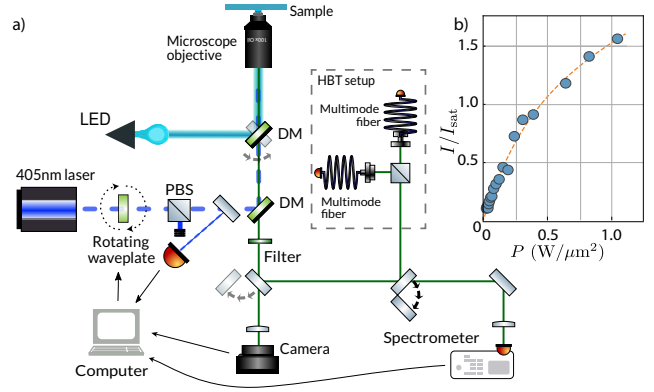


Figure 2: a) Inverted confocal microscope setup for the sample analysis. The emitters can be excited with a LED or a pulsed laser. The emission can be detected on a camera or analyzed with a spectrometer. Finally, we can perform a $g^{(2)}$ measurement with a Hanbury Brown and Twiss setup (HBT setup), with multimode optical fibers connected to APDs. DM: dichroic mirror, PBS: polarizing beam splitter. b) Saturation measurement of a single NC. The blue dots are the experimental data while the orange line is the fitted function from equation (1).

and 15 nm for the second one. By comparison with the bulk perovskite emission wavelength at about 520 nm,^{24–26} we attribute the former emission to small single photon emitters NCs with slight quantum confinement and the latter emission to large size nanocubes for which the confinement is mostly absent. As shown in the following, the small size nanocubes exhibit strongly antibunched emission, highlighting for the first time in this kind of emitters the crucial role of the charge confinement on their quantum properties. We report a study over 24 different emitters. For each emitter we measured the emitted power as a function of the excitation intensity. The background is subtracted from the experimental data. By fitting the data using the following saturation function, we are able to extract the saturation intensity I_{sat} :

$$P = A \cdot \left[1 - e^{-\frac{I}{I_{sat}}} \right] + B \cdot I \quad (1)$$

The first term of the sum represents the saturating part due to the single exciton component while the second is due to bi-exciton emis-

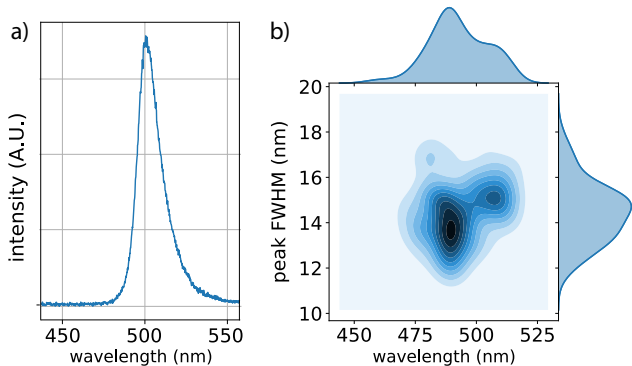


Figure 3: a) Typical emission spectrum of a single NCs and b) central wavelength and FWHM distributions of the emission for a sample of 24 emitters.

sion.^{8,27,28} Specifically I_{sat} is the saturation intensity while A and B depend on the intensity of single and bi-exciton components of the emission.

A typical saturation curve is shown in Figure 2b. To minimize the effect of the blinking on the data analysis, multiple measurements are taken for each experimental intensity in the graph, and only the one with the strongest emission is kept. We observed a median I_{sat} of $0.56 \text{ W}/\mu\text{m}^2$. The presence of a bi-exciton component indicates that the correlation function $g^{(2)}(0)$ will depend on the intensity at which we excite the emitters. We clearly observed this behavior when repeating the measurements for several excitation intensities. To perform reliable measurements on several emitters and to ensure a signal well above the noise level, we performed all the measurements at the saturation intensity.

Effect of the sample dilution on the photobleaching

Usually perovskite nanocrystals at room temperature suffer from fast photo-bleaching when they are exposed to light. Several studies presented lead halide perovskites NCs emission instability.²⁹ Often, the monitoring of the spectral stability over few minutes is used to evaluate the photo-stability,^{8,28} showing that the CEW shifts to more than 10 nm after few tens of seconds for perovskite nanocrystals directly

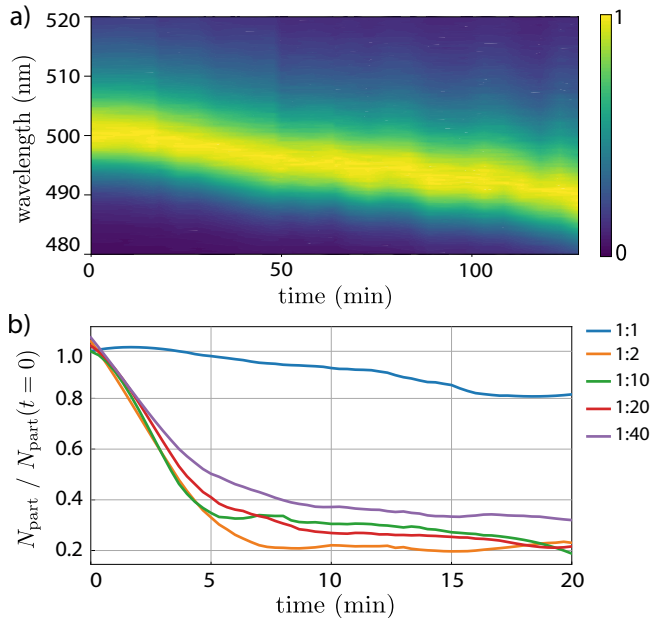


Figure 4: Robustness of perovskites NCs. a) Evolution vs time of the emission wavelength of a single perovskite NC excited at the saturation intensity. Each spectrum is normalized. b) Percentage of NCs still emitting after a certain time under strong illumination as a function of the dilution of the original solution: 1:1, 1:2, 1:10, 1:20, 1:40 where 1:X means x times dilution.

deposited on a glass-plate. Even when they are encapsulated with polystyrene, the longest measurement time recorded in the literature by Rain *et al.*⁸ was around 100 s. The observed spectral drift has been attributed to the degradation of the nanocrystals, resulting in a progressive reduction of their sizes. In our case, the study of the photo-stability of the sample synthesized with the procedure described above shows a significant improvement of the photo-stability of the emitters under illumination. We prepared six samples using different dilutions starting from the most concentrated solution (typically with a molar concentration between $1 \mu\text{M}$ - $10 \mu\text{M}$), up to a dilution of 1:100, using toluene as solvent. We started by analyzing the highest concentration sample. With this concentration value, we are still able to individually address each emitter and to collect its luminescence for more than 1 h with strongly reduced bleaching effects. This can be clearly see in Figure 4a: an emitter is excited for 2 h while

its emission spectrum is collected every 5 min. The figure reports the evolution of the normalized emission spectra versus time. A blue-shift is observed, as already reported by Rain *et al.*,⁸ but on a much longer time scale: indeed our emitters exhibit a blue-shift of less than 10 nm after two hours, showing a remarkable stability, two orders of magnitude better than previously observed.^{5,8} To the best of our knowledge, it is one of the most robust samples reported in the literature.

This robustness is strongly related to the concentration of the emitters in the solution, and drops fast when we dilute the sample. Our final objective is to couple a single emitter to a tapered optical nanofiber to develop an integrated single photon source. For this, we need to use a strongly diluted sample. It is then crucial to investigate the behavior of the emitters as a function of the concentration.

The results of a systematic study of the effect of the dilution are reported in Figure 4b where each sample is strongly illuminated with light from the LED lamp while a video of the sample emission is recorded. Analyzing each frame of the video (we take a frame each 20 seconds) we can estimate the number of NCs that are still emitting from the first frame. We can clearly see that only the concentrated sample (so-called (1:1)) lasts for a long time with more than 80% of the emitters still working after 20 min, while for all the other samples (from dilutions (1:2) to (1:100)) half of the emitters have bleached after 3 min. We attribute this effect to the dynamic bonding of the ligand to the perovskite nanocrystal surface. Under dilute conditions, the free ligands can hardly find the surface of another nanocrystal. This displaces the equilibrium between bound and unbound ligands towards the latter. As a result, the dilution process leads to poorly passivated nanocrystals which can easily bleach.

Blinking characterization

The emitted intensity of a NC is not constant in time but tends to fluctuate: this phenomenon is known as blinking. This behavior has been reported for several kinds of quantum emitters

such as single molecules,^{30,31} Si nanocrystals³² and CdSe/CdS colloidal quantum dots.^{33–38}

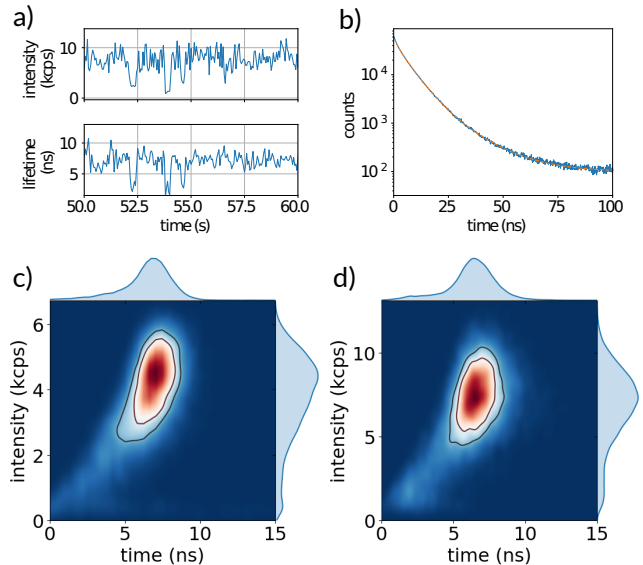


Figure 5: (a) Blinking trace (upper graph) and lifetime (lower graph) of a single NC. (b) Lifetime of a single NC, fitted with a triple-exponential decay model. We obtain 1.4 ns, 6.1 ns and 14.7 ns, corresponding respectively to the lifetimes of the biexciton, grey and neutral emission states. (c,d) Fluorescence lifetime-intensity distribution (FLID) images of a single emitter, excited at half (c) and twice (d) the saturation intensity. The closed curves contains 50% (inner one) and 68% (outer one) of the occurrences.

Usually the fluorescence blinking is attributed to the trapping of charge carriers. In particular, it has been shown that we can distinguish two types of blinking: Type A, in which the core is left effectively charged and the low fluorescence state is caused by the recombination due to the Auger effect, and Type B, in which the trapped charge can recombine non-radiatively with its opposite charge and the blinking is due to fluctuations in the trapping rate.

A well established method to experimentally distinguish between Type A and Type B blinking is to study the spontaneous emission lifetime dependence on the emission intensity: in Type A blinking the lifetime is expected to depend on the emission intensity³⁹ while in Type B the lifetime should not depend on the intensity.^{39,40}

When the typical blinking time is too short with respect to the chosen binning of the time-trace curve, it becomes impossible to completely distinguish between grey and bright states: in this case it is more appropriate to describe the behavior of the emitter in terms of flickering.³⁹

Our emitters, like the vast majority of perovskite NCs reported in the literature,^{41,42} show a clear flickering behavior in their emission time trace. A zoom of a typical blinking trace (i.e. the emitted intensity as a function of time) of one emitter is shown in the upper box of Figure 5a. The signal is binned with a binning time of 50 ms. The complete blinking trace is reported in the supplementary information. Interestingly, the inspection of this trace indicates a reduced blinking with respect to the typical behavior of this kind of perovskites reported in literature.⁵ In the lower box of Figure 5a the mean lifetime versus time is reported: a clear correlation between the two curves is observable which indicates the presence of a type A blinking for these emitters.

In order to perform a more quantitative analysis, we fit the lifetime histogram with a triple-exponential decay model:

$$A_1 \cdot e^{-\frac{t-t_0}{\tau_1}} + A_2 \cdot e^{-\frac{t-t_0}{\tau_2}} + A_3 \cdot e^{-\frac{t-t_0}{\tau_3}} + B \quad (2)$$

with three different lifetimes, τ_1 , τ_2 and τ_3 , corresponding to the neutral, the charged, and the biexciton state emission respectively.³⁹ In equation (2) t_0 represents the pulse arrival time, while A_i are the amplitudes of each decay component; B is an offset added to take into account the dark counts. A typical result of the fitting procedure is shown in Figure 5b, showing a good agreement with the experimental results. The dependence of the lifetime on the emitted intensity is commonly studied^{5,39,43} by using the fluorescence lifetime-intensity distribution (FLID). In Figure 5c and 5d two FLIDs images corresponding to the same NC are shown, corresponding to an excitation intensity of $0.5I_{sat}$ and $2I_{sat}$ respectively, obtained with a bin size of 50 ms. The dark curves delimit an area corresponding respectively to 50% (inner one) and 68% (outer one) probability of emission. As

opposed to previous reports,⁵ showing a predominance of the grey state emission for high excitation powers, with a significant decrease of the emission intensity, remarkably, our perovskite nanocubes remain in the same proportion of bright and grey state while excited up to $2I_{sat}$ and more, without any significant decrease of the emission intensity.

Quantum properties

To characterize the quantum emission and verify if our NCs can be used as single photon emitters, we measured the autocorrelation function $g^{(2)}$ using a Hanbury Brown and Twiss (HBT) setup (see Figure 2). The autocorrelation function is defined as follows:

$$g^{(2)}(\tau) = \frac{\langle I(t)I(t+\tau) \rangle}{\langle I(t) \rangle^2},$$

where I is the intensity of the emission, t the time and τ the delay between two different photon arrivals.

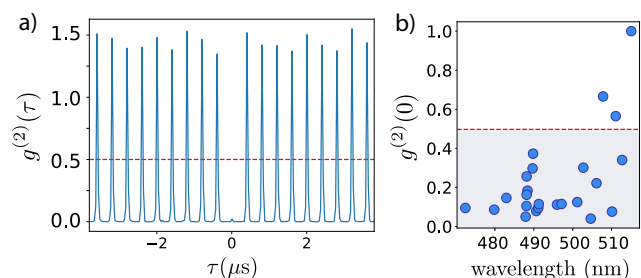


Figure 6: a) Example of $g^{(2)}$ function of a single NC emitting high quality single photons, measured with a repetition rate of 2.5 MHz b) Measured $g^{(2)}(0)$ values as a function of the central wavelength of the emission of the NC. All the emitters were excited at their saturation intensity.

Experimentally the beam is divided in two parts by a 50/50 beam splitter (see Figure 2a) and sent to two avalanche photodiode single photon detectors (APDs). We record the arrival times with the time tagged time-resolved⁴⁴ method. We then create a histogram of the relative arrival times of the photons with a time bin of 18 ns, shown in figure 6a. Due to the blinking effect, the peaks close to the 0 delay

peak are higher than 1;⁴⁵ on the other hand the peaks of the autocorrelation function tend to 1 for large delays compared to the characteristic blinking time. The histogram is thus normalized by setting the mean height of the peaks with $\tau \approx 10 \mu\text{s}$ to be 1. This procedure is well established and documented in literature.^{46,47} The background, mainly given by the dark counts of the APDs, is subtracted following the procedure described in supplementary materials.

The $g^{(2)}$ at $\tau = 0$ delay is 0.02 according to Figure 6a, well below 0.5 showing clear signature of a single photon emission. We found that 50% of our emitters show a very good single photon emission, with $g^{(2)}(\tau) < 0.2$.

We perform a statistical analysis of the $g^{(2)}(0)$ as a function of the central emission wavelength, shown in Figure 6b. We observe a clear degradation of the single photon emission for longer wavelengths. In particular, for CEWs above 505 nm, the autocorrelation function value is always higher than 0.5, indicating that the single photon emission is lost. The reason for that is that for the biggest NCs the quantum confinement is no longer effective and this has the effect to increase the emission wavelength and to reduce the quality of the single photon emission.

Nanofiber integration

In this section, we describe the first realization of the coupling of a single perovskite nanocube with an optical tapered nanofiber, constituting a prototype of an interesting hybrid nanophotonic device for quantum technologies-oriented applications. Tapered nanofibers are photonic waveguides obtained by stretching a standard optical fiber while heating it, in order to reduce its diameter to some hundreds of nanometers. This results in a strong evanescent field in the vicinity of the fiber,⁴⁸ which enables the coupling of the light emitted by a nano-emitter located nearby directly into the nanofiber thus obtaining a compact and integrated single photon source.⁴⁹ This approach has been demonstrated with single atoms^{12,13} as well as single

colloidal quantum dots^{14–16} or with nanodiamonds containing single NV^- defects.¹⁷ This is of great interest for quantum applications, where nanofiber-based systems are rapidly developing.⁵⁰

In order to couple our NCs to the nanofiber, we place on top of it a 20 μL droplet with a dilution 1:100 of the original solution in toluene using a micropipette. We then use a translation stage to carefully approach and eventually touch the nanofiber with the droplet, while monitoring the movement with a microscope. This is a critical step, as the nanofiber can easily break. When successful, this procedure results in several emitters deposited onto the nanofiber.

The setup used for this study is shown in Figure 7. We firstly select the emitter send-

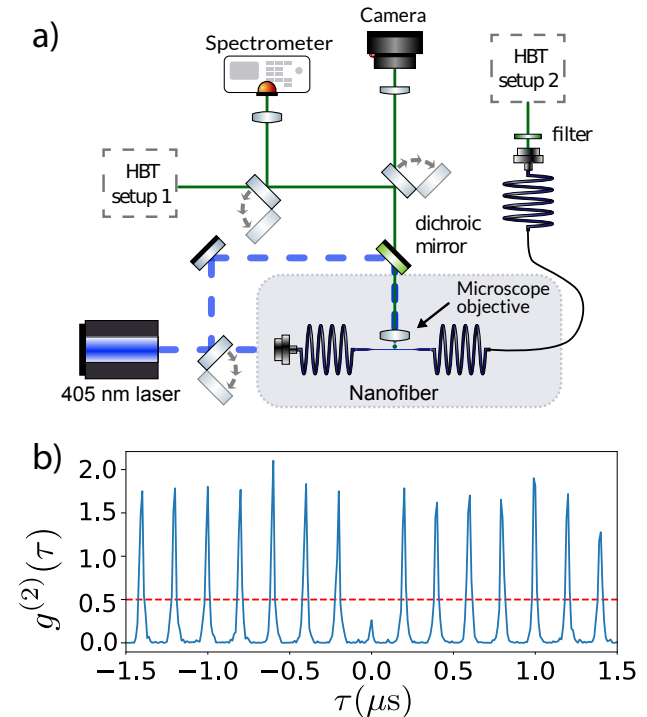


Figure 7: a) Setup used to measure single photons emission from a NC coupled to the nanofiber. b) $g^{(2)}$ function of a single NC emitting single photons into the nanofiber (HBT setup 2 of figure a), measured with a repetition rate of 5 MHz.

ing the laser in the fiber and detect the photoluminescence from the microscope objective. Then, we excite a single NC located on top of the nanofiber with a laser sent through that mi-

croscope objective. A significant fraction of the emitted light is coupled into the nanofiber and propagates to its end. The end of the fiber is plugged to an HBT set-up for a $g^{(2)}$ measurement following the procedure previously described. Optionally, photon antibunching and spectral measurements can be performed also in free-space via the light collected with the microscope objective. A typical antibunching measurement performed on the light collected via the nanofiber is shown in Figure 7. We are still able to detect single photon emission, and this demonstrates that a single perovskite NC is coupled to a nanofiber and emits single photons directly inside it. These results show that our NCs are not damaged by the deposition process and validate this approach for this kind of sources, that, due to the dilution, can be used for some minutes once deposited over the nanofiber. Due to the versatility of the perovskite nanocubes and to their emission of single photons with long coherence time,² this technique opens the way to the realization of nanofiber-based, compact, integrated hybrid devices for indistinguishable single photon generation with solid state emitters. In order to achieve this final goal, it is crucial to further improve the stability of the emitters thanks to a deeper understanding of the role that ligands and dilution play on their robustness.

Conclusions

We investigated the properties of highly-stable CsPbBr₃ nanocrystals as single photon emitters. The effect of the dilution on the photostability was investigated, confirming a degradation when increasing the dilution. To further improve the stability, a promising approach, currently under investigation, is based on a better ligand control in order to increase the dilution without breaking the equilibrium of the colloidal solution.

A full characterization of the optical properties of these emitters was performed, highlighting the role of the charge confinement in their antibunching behaviour. A deep analysis of the blinking and single photon emission

of perovskite nanocubes were presented, showing a strongly reduced blinking and a remarkable stability of the bright state emission as a function of the excitation power. This feature guarantees a very low $g^{(2)}(0)$ also for high excitation power. Moreover, for the first time with such emitters, we have shown the coupling of a single perovskite nanocube with a tapered optical nanofiber. Thanks to the near-field interaction, single photons are emitted in the near field of the nanofiber demonstrating the proof of principle of a compact, integrated single photon source. The coupling to other platforms, such as the ion-integrated waveguides one,⁵¹ is also envisioned to obtain integrated single photon sources for quantum photonic applications.

Experimental

Chemicals

PbBr₂ (Alfa Aesar, 98.5%), Cs₂CO₃ (Alfa aesar, 99,99%), oleylamine (OLA, Acros, 80 – 90%), oleic acid (OA, Sigma-Aldrich), octylamine (Oct.Am, Alfa aesar, 99%), Octanoic acid (Oct.Acid, Acros, 99%), octadecene (ODE, Acros Organics, 90%), toluene (VWR, rechapur).

Caesium oleate precursor

We mix in a 50 mL three neck flask, 350 mg of Cs₂CO₃ in 20 mL of ODE and 1.25 mL of OA. The content of the flask is stirred and degased under vacuum at room temperature for 25 min. The flask is heated at 110 °C for 15 min. The atmosphere is switched to nitrogen and the temperature raised to 150 °C. The reaction is carried on for 15 min. At this stage the salt is fully dissolved. The temperature is cooled down below 100 °C and the flask degased under vacuum. Finally this solution is used as a stock solution.

Nanocrystal synthesis

In a three neck flask, 174 mg of PbBr₂ is mixed in 10 mL of ODE. The flask is degased under vacuum at room temperature for 15 min. Then, the temperature is raised to 120 °C. At 105 °C,

0.25 mL of OLA is injected. Once vacuum has recovered, 1.1 mL of OA is injected. After 5 min, 0.75 mL of oct.Am is injected. Once the vacuum has recovered, 0.75 mL of oct.Acid is injected. The solution is colorless at this stage. The solution is further degased at 120 °C for 30 min. The atmosphere is switched to nitrogen and the temperature raised to 150 °C. Around 0.1 mL of CsOA solution is injected, and the solution turns turbid. The solution is conducted for 35 min and finally quickly cooled down by removing the heating mantle and using a water bath. The solution is transferred to plastic tube and centrifuged. The supernatant is discarded. The pellet is dispersed in 5 mL of toluene. The solution is centrifuged again at low speed (2000 rpm for 1 min). The pellet is discarded and the colloidally stable supernatant is stored.

Material characterization

UV-visible absorption spectrum are obtained by diluting the nanoparticles in hexane and using a JASCO V730 spectrometer. For transmission electron microscopy, a dilute solution of nanocrystals is drop-casted onto a copper grid coated with a thin amorphous carbon layer. The grid is then degased under secondary vacuum overnight. Imaging was conducted with a JEOL 2010 microscope operated at 200 kV.

Acknowledgement The project is supported by ERC starting grant blackQD (grant n 756225), by ANR grants IPER-Nano2 (ANR-18CE30-0023-01), Copin (ANR-19-CE24-0022), Frontal (ANR-19-CE09-0017), Graskop (ANR-19-CE09-0026) and by the European Unions Horizon 2020 research and innovation program under grant agreement No 828972 -Nanobright. AB and QG are members of the Institut Universitaire de France (IUF). The authors thank J.-P. Hermier for inspiring discussions.

Supporting Information Available

The following files are available free of charge.

Supporting information available: Integral fluorescence trace, procedure for FLID generation, noise cleaning procedure for $g^{(2)}(\tau)$ measurements, procedure for NCs deposition on nanofibers. This material is available free of charge via the internet at <http://pubs.acs.org>

References

1. Park, N.-G. Perovskite solar cells: an emerging photovoltaic technology. *Materials today* **2015**, *18*, 65–72.
2. Utzat, H.; Sun, W.; Kaplan, A. E. K.; Krieg, F.; Ginterseder, M.; Spokoiny, B.; Klein, N. D.; Shulenberger, K. E.; Perkinson, C. F.; Kovalenko, M. V. *et al.* Coherent Single-Photon Emission from Colloidal Lead Halide Perovskite Quantum Dots. *Science* **2019**, *363*, 1068–1072.
3. Rainò, G.; Nedelcu, G.; Protesescu, L.; Bodnarchuk, M. I.; Kovalenko, M. V.; Mahrt, R. F.; Stöferle, T. Single Cesium Lead Halide Perovskite Nanocrystals at Low Temperature: Fast Single-Photon Emission, Reduced Blinking, and Exciton Fine Structure. *ACS Nano* **2016**, *10*, 2485–2490.
4. Huo, C.; Fong, C. F.; Amara, M.-R.; Huang, Y.; Chen, B.; Zhang, H.; Guo, L.; Li, H.; Huang, W.; Diederichs, C. *et al.* Optical Spectroscopy of Single Colloidal CsPbBr₃ Perovskite Nanoplatelets. *Nano Letters* **2020**,
5. Park, Y.-S.; Guo, S.; Makarov, N. S.; Klimov, V. I. Room Temperature Single-Photon Emission from Individual Perovskite Quantum Dots. *ACS Nano* **2015**, *9*, 10386–10393.
6. Rainò, G.; Becker, M. A.; Bodnarchuk, M. I.; Mahrt, R. F.; Kovalenko, M. V.; Stöferle, T. Superfluorescence from Lead Halide Perovskite Quantum Dot Superlattices. *Nature* **2018**, *563*, 671–675.

7. Chen, L.-C.; Tien, C.-H.; Tseng, Z.-L.; Dong, Y.-S.; Yang, S. Influence of PMMA on All-Inorganic Halide Perovskite CsPbBr₃ Quantum Dots Combined with Polymer Matrix. *Materials* **2019**, *12*, 985.
8. Rain, G.; Landuyt, A.; Krieg, F.; Bernasconi, C.; Ochsenbein, S. T.; Dirin, D. N.; Bodnarchuk, M. I.; Kovalenko, M. V. Underestimated Effect of a Polymer Matrix on the Light Emission of Single CsPbBr₃ Nanocrystals. *Nano Letters* **2019**, *19*, 3648–3653.
9. Saris, S.; Dona, S.; Niemann, V.; Loiudice, A.; Buonsanti, R. Optimizing the Atomic Layer Deposition of Alumina on Perovskite Nanocrystal Films by Using O₂ as a Molecular Probe. *ChemRxiv* **2019**,
10. Xiang, Q.; Zhou, B.; Cao, K.; Wen, Y.; Li, Y.; Wang, Z.; Jiang, C.; Shan, B.; Chen, R. Bottom up Stabilization of CsPbBr₃ Quantum Dots-Silica Sphere with Selective Surface Passivation via Atomic Layer Deposition. *Chemistry of Materials* **2018**, *30*, 8486–8494.
11. Pan, J.; Sarmah, S. P.; Murali, B.; Dursun, I.; Peng, W.; Parida, M. R.; Liu, J.; Sinatra, L.; Alyami, N.; Zhao, C. *et al.* Air-Stable Surface-Passivated Perovskite Quantum Dots for Ultra-Robust, Single- and Two-Photon-Induced Amplified Spontaneous Emission. *The Journal of Physical Chemistry Letters* **2015**, *6*, 5027–5033.
12. Le Kien, F.; Gupta, S. D.; Balykin, V.; Hakuta, K. Spontaneous emission of a cesium atom near a nanofiber: Efficient coupling of light to guided modes. *Physical Review A* **2005**, *72*, 032509.
13. Klimov, V.; Ducloy, M. Spontaneous emission rate of an excited atom placed near a nanofiber. *Physical Review A* **2004**, *69*, 013812.
14. Fujiwara, M.; Toubaru, K.; Noda, T.; Zhao, H.-Q.; Takeuchi, S. Highly efficient coupling of photons from nanoemitters into single-mode optical fibers. *Nano letters* **2011**, *11*, 4362–4365.
15. Yalla, R.; Nayak, K.; Hakuta, K. Fluorescence photon measurements from single quantum dots on an optical nanofiber. *Optics express* **2012**, *20*, 2932–2941.
16. Joos, M.; Ding, C.; Loo, V.; Blanquer, G.; Giacobino, E.; Bramati, A.; Krachmalnicoff, V.; Glorieux, Q. Polarization control of linear dipole radiation using an optical nanofiber. *Physical Review Applied* **2018**, *9*, 064035.
17. Vorobyov, V. V.; Soshenko, V. V.; Bolshedvorskii, S. V.; Javadzade, J.; Lebedev, N.; Smolyaninov, A. N.; Sorokin, V. N.; Aki-mov, A. V. Coupling of Single NV Center to Adiabatically Tapered Optical single Mode Fiber. *The European Physical Journal D* **2016**, *70*, 269.
18. Protesescu, L.; Yakunin, S.; Bodnarchuk, M. I.; Krieg, F.; Caputo, R.; Hendon, C. H.; Yang, R. X.; Walsh, A.; Kovalenko, M. V. Nanocrystals of cesium lead halide perovskites (CsPbX₃, X= Cl, Br, and I): novel optoelectronic materials showing bright emission with wide color gamut. *Nano letters* **2015**, *15*, 3692–3696.
19. De Roo, J.; Ibáñez, M.; Geiregat, P.; Nedelcu, G.; Walravens, W.; Maes, J.; Martins, J. C.; Van Driessche, I.; Kovalenko, M. V.; Hens, Z. Highly dynamic ligand binding and light absorption coefficient of cesium lead bromide perovskite nanocrystals. *ACS nano* **2016**, *10*, 2071–2081.
20. Krieg, F.; Ong, Q. K.; Burian, M.; Rainò, G.; Naumenko, D.; Amenitsch, H.; Süess, A.; Grotevent, M. J.; Krumeich, F.; Bodnarchuk, M. I. *et al.* Stable Ultra-concentrated and Ultradilute Colloids of CsPbX₃ (X= Cl, Br) Nanocrystals Using Natural Lecithin as a Capping Ligand. *Journal of the American Chemical Society* **2019**, *141*, 19839–19849.

21. Zhang, B.; Goldoni, L.; Zito, J.; Dang, Z.; Almeida, G.; Zaccaria, F.; De Wit, J.; Infante, I.; De Trizio, L.; Manna, L. Alkyl phosphonic acids deliver CsPbBr₃ Nanocrystals with high photoluminescence quantum yield and truncated octahedron shape. *Chemistry of Materials* **2019**, *31*, 9140–9147.
22. Liu, Y.; Siron, M.; Lu, D.; Yang, J.; dos Reis, R.; Cui, F.; Gao, M.; Lai, M.; Lin, J.; Kong, Q. *et al.* Self-Assembly of Two-Dimensional Perovskite Nanosheet Building Blocks into Ordered Ruddlesden–Popper Perovskite Phase. *Journal of the American Chemical Society* **2019**, *141*, 13028–13032.
23. Weidman, M. C.; Seitz, M.; Stranks, S. D.; Tisdale, W. A. Highly tunable colloidal perovskite nanoplatelets through variable cation, metal, and halide composition. *ACS nano* **2016**, *10*, 7830–7839.
24. Mannino, G.; Deretzis, I.; Smecca, E.; La Magna, A.; Alberti, A.; Ceratti, D.; Cahen, D. Temperature-Dependent Optical Band Gap in CsPbBr₃, MAPbBr₃, and FAPbBr₃ Single Crystals. *The Journal of Physical Chemistry Letters* **2020**, *11*, 2490–2496.
25. Liashenko, T. G.; Cherotchenko, E. D.; Pushkarev, A. P.; Pakštas, V.; Naujokaitis, A.; Khubezhov, S. A.; Polozkov, R. G.; Agapev, K. B.; Zakhidov, A. A.; Shelykh, I. A. *et al.* Electronic structure of CsPbBr_{3-x}Cl_x perovskites: synthesis, experimental characterization, and DFT simulations. *Physical Chemistry Chemical Physics* **2019**, *21*, 18930–18938.
26. Ng, C. H.; Ripolles, T. S.; Hamada, K.; Teo, S. H.; Lim, H. N.; Bisquert, J.; Hayase, S. Tunable open circuit voltage by engineering inorganic cesium lead bromide/iodide perovskite solar cells. *Scientific reports* **2018**, *8*, 1–9.
27. Park, Y.-S.; Malko, A. V.; Vela, J.; Chen, Y.; Ghosh, Y.; García-Santamaría, F.; Hollingsworth, J. A.; Klimov, V. I.; Htoon, H. Near-unity quantum yields of biexciton emission from CdSe/CdS nanocrystals measured using single-particle spectroscopy. *Physical review letters* **2011**, *106*, 187401.
28. Raja, S. N.; Bekenstein, Y.; Koc, M. A.; Fischer, S.; Zhang, D.; Lin, L.; Ritchie, R. O.; Yang, P.; Alivisatos, A. P. Encapsulation of Perovskite Nanocrystals into Macroscale Polymer Matrices: Enhanced Stability and Polarization. *ACS Applied Materials & Interfaces* **2016**, *8*, 35523–35533.
29. Huang, H.; Bodnarchuk, M. I.; Kershaw, S. V.; Kovalenko, M. V.; Rogach, A. L. Lead Halide Perovskite Nanocrystals in the Research Spotlight: Stability and Defect Tolerance. *ACS Energy Letters* **2017**, *2*, 2071–2083.
30. Yip, W.-T.; Hu, D.; Yu, J.; Vandenberg, D. A.; Barbara, P. F. Classifying the Photophysical Dynamics of Single- and Multiple-Chromophoric Molecules by Single Molecule Spectroscopy. *The Journal of Physical Chemistry A* **1998**, *102*, 7564–7575.
31. Dickson, R. M.; Cubitt, A. B.; Tsien, R. Y.; Moerner, W. E. On/off Blinking and Switching Behaviour of Single Molecules of Green Fluorescent Protein. *Nature* **1997**, *388*, 355–358.
32. Mason, M. D.; Credo, G. M.; Weston, K. D.; Buratto, S. K. Luminescence of Individual Porous Si Chromophores. *Physical Review Letters* **1998**, *80*, 5405–5408.
33. Nirmal, M.; Dabbousi, B. O.; Bawendi, M. G.; Macklin, J. J.; Trautman, J. K.; Harris, T. D.; Brus, L. E. Fluorescence Intermittency in Single Cadmium Selenide Nanocrystals. *Nature* **1996**, *383*, 802–804.

34. Shimizu, K. T.; Neuhauser, R. G.; Leatherdale, C. A.; Empedocles, S. A.; Woo, W. K.; Bawendi, M. G. Blinking Statistics in Single Semiconductor Nanocrystal Quantum Dots. *Physical Review B* **2001**, *63*, 205316.
35. Tang, J.; Marcus, R. A. Single Particle versus Ensemble Average: From Power-Law Intermittency of a Single Quantum Dot to Quasistretched Exponential Fluorescence Decay of an Ensemble. *The Journal of Chemical Physics* **2005**, *123*, 204511.
36. Peterson, J. J.; Nesbitt, D. J. Modified Power Law Behavior in Quantum Dot Blinking: A Novel Role for Biexcitons and Auger Ionization. *Nano Letters* **2009**, *9*, 338–345.
37. Mahler, B.; Spinicelli, P.; Buil, S.; Quelin, X.; Hermier, J.-P.; Dubertret, B. Towards Non-Blinking Colloidal Quantum Dots. *Nature Materials* **2008**, *7*, 659–664.
38. Houel, J.; Doan, Q. T.; Cajgffinger, T.; Ledoux, G.; Amans, D.; Aubret, A.; Dominjon, A.; Ferriol, S.; Barbier, R.; Nasilowski, M. *et al.* Autocorrelation Analysis for the Unbiased Determination of Power-Law Exponents in Single-Quantum-Dot Blinking. *ACS Nano* **2015**, *9*, 886–893.
39. Galland, C.; Ghosh, Y.; Steinbrück, A.; Sykora, M.; Hollingsworth, J. A.; Klimov, V. I.; Htoon, H. Two types of luminescence blinking revealed by spectroelectrochemistry of single quantum dots. *Nature* **2011**, *479*, 203–207.
40. Brawand, N. P.; Vörös, M.; Galli, G. Surface Dangling Bonds Are a Cause of B-Type Blinking in Si Nanoparticles. *Nanoscale* **2015**, *7*, 3737–3744.
41. Trinh, C. T.; Minh, D. N.; Ahn, K. J.; Kang, Y.; Lee, K.-G. Organic-Inorganic FAPbBr₃ Perovskite Quantum Dots as a Quantum Light Source: Single-Photon Emission and Blinking Behaviors. *ACS Photonics* **2018**, *5*, 4937–4943.
42. Seth, S.; Mondal, N.; Patra, S.; Samanta, A. Fluorescence Blinking and Photoactivation of All-Inorganic Perovskite Nanocrystals CsPbBr₃ and CsPbBr₂I. *The Journal of Physical Chemistry Letters* **2016**, *7*, 266–271.
43. Hu, F.; Cao, Z.; Zhang, C.; Wang, X.; Xiao, M. Defect-Induced Photoluminescence Blinking of Single Epitaxial InGaAs Quantum Dots. *Scientific Reports* **2015**, *5*, 1–6.
44. Wahl, M.; Orthaus-Müller, S. Time tagged time-resolved fluorescence data collection in life sciences. *technical note, PicoQuant GmbH* **2014**,
45. Manceau, M.; Vezzoli, S.; Glorieux, Q.; Giacobino, E.; Carbone, L.; De Vittorio, M.; Hermier, J.-P.; Bramati, A. CdSe/CdS Dot-in-Rods Nanocrystals Fast Blinking Dynamics. *ChemPhysChem* **2018**, *19*, 3288–3295.
46. Pierini, S.; D’Amato, M.; Joos, M.; Glorieux, Q.; Giacobino, E.; Lhuillier, E.; Couteau, C.; Bramati, A. Hybrid Device for Quantum Nanophotonics. *arXiv:2001.10480 [physics, physics:quant-ph]* **2020**,
47. Manceau, M.; Vezzoli, S.; Glorieux, Q.; Pisanello, F.; Giacobino, E.; Carbone, L.; De Vittorio, M.; Bramati, A. Effect of charging on CdSe/CdS dot-in-rods single-photon emission. *Physical Review B* **2014**, *90*, 035311.
48. Le Kien, F.; Liang, J. Q.; Hakuta, K.; Balykin, V. I. Field Intensity Distributions and Polarization Orientations in a Vacuum-Clad Subwavelength-Diameter Optical Fiber. *Optics Communications* **2004**, *242*, 445–455.
49. Joos, M.; Bramati, A.; Glorieux, Q. Complete polarization control for a nanofiber waveguide using the scattering properties. *Optics express* **2019**, *27*, 18818–18830.

50. Nayak, K. P.; Sadgrove, M.; Yalla, R.; Le Kien, F.; Hakuta, K. Nanofiber quantum photonics. *Journal of Optics* **2018**, *20*, 073001.
51. Madrigal, J. B.; Tellez-Limon, R.; Gardillou, F.; Barbier, D.; Geng, W.; Couteau, C.; Salas-Montiel, R.; Blaize, S. Hybrid integrated optical waveguides in glass for enhanced visible photoluminescence of nanoemitters. *Applied optics* **2016**, *55*, 10263–10268.